15 September 2001

ELSEVIER

Optics Communications 197 (2001) 131–143

OPTICS COMMUNICATIONS

www.elsevier.com/locate/optcom

Femtosecond and picosecond ultraviolet laser filaments in air: experiments and simulations

S. Tzortzakis [a,*], B. Lamouroux [a], A. Chiron [a], S.D. Moustaizis [b], D. Anglos [b], M. Franco [a], B. Prade [a], A. Mysyrowicz [a]

[a] *Laboratoire d'Optique Appliquée, CNRS UMR 7639, ENSTA – Ecole Polytechnique, Chemin de la Hunière, 91761 Palaiseau Cedex, France*

[b] *Foundation for Research and Technology Hellas, Institute of Electronic Structure and Laser, P.O. Box 1527, Heraklion 711 10, Greece*

Received 23 April 2001; accepted 19 July 2001

Abstract

We report a study of the long-range self-guided propagation of intense femtosecond and picosecond UV laser pulses in air. Measurements of the laser beam profile along the propagation axis together with the ionization rate, the pulse temporal profile and power spectrum provide a comprehensive image of the UV filamentation process and its characteristics. Self-guiding is shown to subsist in both fs and ps cases, with a robust filament propagating over several meters in air. Stable filamentation is accompanied by an important restructuring of the pulse temporal profile. Complementary numerical simulations, using a three-dimension propagation code, are compared to the experimental results. The simulations reproduce most experimental observations, allowing for a better understanding of the phenomena involved in this unique propagation mode. © 2001 Published by Elsevier Science B.V.

PACS: 42.65.Tg; 42.65.Jx

Keywords: Nonlinear guided waves; Beam trapping

1. Introduction

Propagation of electromagnetic pulses is of fundamental importance in pure and applied science, and the recent development of sources of intense ultrashort laser pulses has added many interesting twists to this long standing problem. The broad spectral bandwidths, high peak powers, and $(3+1)$-dimensional nature of these fields give rise to complex linear and nonlinear effects that have posed significant challenges to researchers.

In the last years an important effort has been devoted to the study of the propagation of powerful laser beams in atmosphere as well as in other transparent media, i.e. glasses. A particular interest has focused on femtosecond laser systems, able to deliver very high peak powers with a modest energy output. Due to the high power the nonlinear response of the medium plays a key role in the propagation. Complementary to the experiments, the nonlinear propagation is simulated numerically by solving a complex extended

* Corresponding author. Fax: +33-1-6931-9996.
E-mail address: stzortz@enstay.ensta.fr (S. Tzortzakis).

0030-4018/01/$ - see front matter © 2001 Published by Elsevier Science B.V.
PII: S0030-4018(01)01443-2

nonlinear Schrödinger equation (NLS) including: linear diffraction, the optical Kerr effect, plasma generation from multiphoton absorptions (MPA), normal group velocity dispersion (GVD) or even other higher order terms of temporal dispersion.

Beam self-guiding and filamentation using IR femtosecond powerful lasers has been observed and reported by several groups [1–3]. The key role of multiphoton ionization (MPI) has been well identified. Schillinger and Sauerbrey [4] and Tzortzakis et al. [5,6] have measured the electric conductivity of air in the trail of those filaments and provided estimates of the electron density in the filament, with Schillinger giving a lower limit of 10^{12} cm^{-3} and Tzortzakis a mean density between 10^{16} and 10^{17} cm^{-3}. La Fontaine et al. [7] have reported long-range filamentation in excess of 200 m using a laser system providing pulses at 795 nm and duration of 60 fs. They have measured the electron density in the filament, using longitudinal spectral interferometry, and found it to be a few times 10^{16} cm^{-3}. The same group has performed experiments of laser-triggered discharges using a powerful femtosecond IR laser. They have observed long discharges of more than 2.5 m and an important enhancement of the leader propagation speed by a factor of 10 [8].

Talebpour et al. [9] have reported measurements of the photoemission spectrum of N_2 molecules and N_2^+ molecular ions in the filament. By measuring the intensity of the photoemission signal at different distances they were able to trace the laser beam intensity along the propagation axis. In this way they reported on the observation of refocusing, a feature that has been predicted by several numerical simulations [10–12]. The same group has also reported recently [13] a spectroscopic technique to measure the electronic density in gases.

Mlejnek et al. [10] presented numerical simulations of nonlinear pulse propagation in air whereby an initial pulse is formed, absorbed by plasma generation, and subsequently replenished by power from the trailing edge of the pulse. The evolution of the pulse is dynamic, involving the development of a leading-edge pulse that subsequently decays and is replaced by a new pulse. Spatial ring formation around the filament was also reported. The same research group reported recently [14] a real three-dimension (3D) numerical simulation where the introduction of a large laser beam (7 mm) with power more than $35P_{cr}$, where P_{cr} is the critical power for self-focusing, leads to multibreak-up and multifilamentation. Aközbek et al. [15] provided an alternative analytical method for describing the properties of the femtosecond pulse propagation in air. They approach the plasma generation as an effective higher order $\chi^{(n)}$-like effect. This method reproduced part of the more complex numerical simulations and was in good qualitative agreement with several experimental results.

Koprinkov et al. [16] have recently reported on the existence of spatio-temporal solitons when intense femtosecond laser pulses propagate in gases under high pressure or even transparent solids such as fused silica. Bergé and Couairon have obtained recently a numerical confirmation of a spatio-temporal soliton propagating in atmosphere over a distance of about 60 m [17].

Recently Schwarz et al. [18] and Tzortzakis et al. [19] reported on the filamentation of ultrashort UV laser pulses. In this paper we present a detailed experimental and numeric study on the nonlinear propagation of ultraviolet femtosecond and picosecond laser pulses in air. The comparison between experimental results and the simulations is in most cases very good. We begin in Section 2 with a description of the UV laser system and the experimental techniques used. Then in Section 3 a description of the physical model used in our simulations is given and the numerical procedure followed is described. We provide the reader with all the details relative to the model and the numerical values used. A special effort was made to select the physical parameters known from the current literature and to use initial conditions close to the experimental ones. In Section 4 a detailed presentation of the most important and significant results is given, both experimental and numerical. Laser beam intensity profiles, electron densities, pulse temporal profiles and power spectra at different distances along the laser propagation axis are shown. We report on experimental and numerical evidence of femtosecond and picosecond UV pulse filamentation with long plasma channels and pulse splitting promoted by MPI.

2. Experimental procedure

The UV laser pulses were obtained by doubling the output of a femtosecond dye laser and amplifying it with an Excimer laser amplifier, the whole system operating at a few Hz repetition rate. The laser peak emission wavelength was at 248 nm. The laser could operate either in the fs mode (pulse duration 450 fs and energy per pulse up to 10 mJ) or in the ps mode (5 ps pulse duration and energy per pulse up to 15 mJ). Measurements described here were obtained with both 450 fs and 5 ps long pulses for several input laser energies. The laser beam was directed through a circular diaphragm 7 mm in diameter, and then focused with a lens of focal distance $f = 9.5$ m.

Laser beam profiles were recorded at different propagation distances on UV photographic paper. Filamentation with concomitant plasma channel formation was verified by measuring the electric conductance of air as a function of propagation distance. To detect the presence of a conducting channel, we measure the change of resistivity of air between two electrodes after passage of the filament. All details relative to the electric technique can be found in Ref. [5]. The electron detector was calibrated by means of an optical diffractometry technique described in Ref. [6]. The far field image of a probe beam, modified after the passage through the filament is recorded at different delays. The diffraction patterns obtained in this way are sensitive to the accumulated phase shift, fixing thereby the electron plasma density.

Measurements of the temporal pulse shape were performed using an autocorrelation technique based on the two-photon ionization of NO molecules. A collinear Michelson type interferometer coupled with a cell filled with pure NO molecules at low pressure (typically about 100 mbar) was used [20]. A small part of the laser beam is introduced in the Michelson interferometer from a glass (BK7) plate reflection placed on the laser propagation axis at 45° angle. Measurements were performed only at distances for which the entrance window of the glass plate was not damaged by the laser beam intensity (i.e., outside the focal region) and therefore the reflected beam was not distorted. The free electrons produced from the laser–NO molecules interaction are captured using a system of two electrodes placed in the cell where a moderate potential difference is applied. The signal measured in this way is directly proportional to the number of free electrons produced by the two-photon ionization process of the 248 nm laser radiation used here. The signal measured in this case is proportional to $S(\tau)$ with:

$$S(\tau) = 1 + 2\int I(t)I(t+\tau)\,\mathrm{d}t \Big/ \int I^2(t)\,\mathrm{d}t, \qquad (1)$$

where I is the laser intensity. From the above formula, for $\tau \to \infty$ one has $S(\tau) = 1$, while for $\tau = 0$, $S(\tau) = 3$. Thus the expected ratio of the peak signal to the baseline in the autocorrelation traces is 3. This ratio was an experimental criterion for the validity of the experimental autocorrelation measurements. Fig. 1 (squares and solid line) shows the autocorrelation trace of the initial pulse for the case of fs pulses before propagation, which could be fitted with a sech^2 function (dashed line) with duration of 450 fs, in agreement with the laser specifications.

Spectral measurements of the laser pulse before and after propagation were performed, taking a small reflection of the beam into an $f = 1$ m spectrometer equipped with a 1200 grooves/mm diffraction grating. In some cases another system was used with an $f = 25$ cm spectrometer with a 1200 grooves/mm diffraction grating and a 16 bit linear CCD camera.

Beam profiles and ionization measurements, together with temporal autocorrelations and pulse power spectra were recorded at different propagation

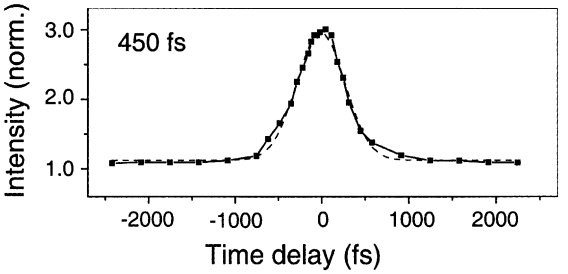

Fig. 1. Measured autocorrelation trace of the initial UV fs pulse before propagation. The dashed line is the fit using a sech^2 function with duration 450 fs.

distances for both fs and ps pulses for several input laser pulse energies.

3. Numerical approach

The propagation of an intense femtosecond laser pulse in a gas involves linear diffraction, linear and nonlinear refraction as well as ionization of air molecules. Much numerical simulation effort has been devoted during the last years to reproduce the experimental observations of the filamentation of intense ultrashort IR laser pulses as well as to provide some predictions, see e.g. Refs. [10–12,21, 22]. For a numerical code to be reliable for predictions, it has to be able, at least, to reproduce most experimental observations by employing realistic physical parameters and initial conditions close to the experimental ones.

Here the experimental results are compared to numerical simulations, using a 3D propagation code with axial symmetry. This code has been successfully applied before to the nonlinear propagation of IR [11] and UV [19] fs laser pulses. This code solves numerically the NLS equation, coupled with the density of electrons produced by MPI. We assume that the beam is linearly polarized with the central frequency ω_0 ($\lambda_0 = 248$ nm) and wave number $k_0 = \omega_0/c$. The pulse has the radial symmetry and its complex envelope $\mathscr{E}(r,t,z)$ evolves according to

$$2\mathrm{i}\frac{\partial \mathscr{E}}{\partial z} + \frac{1}{k_0}\Delta_\perp \mathscr{E} + k_0 n_2 |\mathscr{E}|^2 \mathscr{E} - k_0 \frac{\omega_{\mathrm{pe}}^2(\rho)}{\omega_0^2}\mathscr{E} + \mathrm{i}\sum_m \beta^{K_m} |\mathscr{E}|^{2K_m - 2}\mathscr{E} = 0, \tag{2}$$

$$\frac{\partial \rho}{\partial t} = \sum_m \frac{\beta^{K_m}}{K_m \hbar \omega_0} |\mathscr{E}|^{2K_m} \left(1 - \frac{\rho_m}{\rho_{\mathrm{at}}}\right). \tag{3}$$

This is a multispecies code and here, in the case of air, it treats O_2 and N_2 molecules in the density proportion 20% and 80% respectively. In Eqs. (2) and (3) m represents the two species and K is the respective number of photons needed in the MPI processes that is 3 for O_2 ($U_i = 12.06$ eV) and 4 for N_2 ($U_i = 15.58$ eV). $\rho = \rho_{O_2} + \rho_{N_2}$ is the plasma electron density, while $\rho_{\mathrm{at}} = 2.7 \times 10^{19}$ cm^{-3} is the background atom density satisfying the relation $\rho/\rho_{\mathrm{at}} \leqslant 1\%$. The second term of Eq. (2) describes diffraction in the transverse plane, followed by the Kerr self-focusing with nonlinear refraction index $n_2 = 8 \times 10^{-19}$ cm^2/W, plasma defocusing, excited by MPI, that involves the electron density entering in the plasma frequency $\omega_{\mathrm{pe}}^2(\rho) = q_{\mathrm{e}}^2 \rho / m_{\mathrm{e}} \varepsilon_0$, with q_{e} and m_{e} being the charge and mass of the electron and ε_0 the dielectric constant in vacuum and the related MPA with coefficients β^{K_m}.

Depending on the laser intensity the creation of free electrons is described by one of the following models: the MPI model or the tunnel ionization model. The separation between these regimes is given by the Keldysh constant Γ defined by [22]: $\Gamma_k = [U_k/2\mathscr{V}]^{1/2}$, where U_k is the ionization potential of one atom and $\mathscr{V}$ the quiver energy of the free electron in the laser field; $\mathscr{V} = eE^2/4m_{\mathrm{e}}\omega_0^2$. The multiphoton regime dominates when U_k is much larger than the quiver energy, which corresponds to $\Gamma > 1$. For the intensities considered in this study, $<10^{12}$ W/cm^2, we are placed in the multiphoton regime. The MPA coefficients read as $\beta^3 \simeq 2.14 \times 10^{-32}$ m^3/W^2 and $\beta^4 \simeq 1.13 \times 10^{-50}$ m^5/W^3 for oxygen and nitrogen molecules respectively. These coefficients are calculated based on the Keldysh formulation [23] as analyzed in Ref. [11].

Eq. (2) is solved numerically using a Crank–Nicholson scheme which is an implicit finite-difference method recognized as condition less stable. The continuous field $\mathscr{E}(r,t,z)$ is represented on a regular grid with mesh size Δz and Δr along the axial and transverse directions respectively. The time evolution t is segmented into k elements t_k. The Crank–Nicholson scheme is applied to each time element. As initial conditions, we consider input beams having a spatial super-Gaussian shape (simulating the diaphragm used in the experiments) with a transverse waist of $w_0 = 3$ mm. The temporal profile was assumed of the form of a sech^2 pulse with $\tau_0 = 450$ fs or $\tau_0 = 5$ ps. The beam convergence corresponds to the experimental situation, where a lens with focal length $f = 9.5$ m was used. We did not include in our calculations the retarded Kerr effect. This approximation is justified by the fact that the laser spectrum did not exhibit significant spectral shift to lower energies in

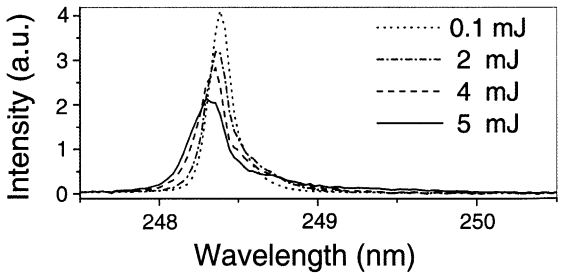

Fig. 2. Measured pulse power spectra of fs UV pulses recorded after 30 m of free propagation in air. In this figure spectra are shown for different input laser pulse energies. They show a small broadening but no global shift of the center of gravity.

the ionization-free region before the focus. This is demonstrated in Fig. 2 where the power spectra of the laser pulse (fs case) are recorded for different input energies after free propagation (collimated beam) over 30 m in air. The absence of a red shift in the first spectral moment indicates that the noninstantaneous Kerr response is small and can be neglected [24]. We also neglect the effect of the GVD as we deal with pulses, which have rather long duration and we are interested in the propagation over relatively short distances (typically several meters).

4. Propagation of ultraviolet short pulses in air

4.1. Spatial characteristics

Fluence diagrams of the spatial evolution of the laser beam as result from the simulations are shown in Fig. 3. The column on the left presents results on 450 fs long pulses while the column on the right presents results for 5 ps long pulses, the first row is for input pulse energy of 2 mJ, the second row for 5 mJ and the third for 7.5 mJ. From those figures the main stages in the propagation can be clearly recognized, showing in all cases the existence of a filament. First the beam self-focuses because of the nonlinear Kerr effect with the nonlinear focus being at about 7.25 m. In this first stage one observes the formation of rings merging inwards to the beam center. Those rings are less pronounced in the case of ps pulses than in the case of fs pulses. As the input energy increases the rings become more perceptible. Another characteristic especially noticeable in the case of fs pulses is the rapid reduction of the fluence in the first meter of propagation. This is due to losses from MPA as we will see later. The filament emerges from the nonlinear focus and propagates on for about 4 m subject to radiation losses. Rings merging outwards surround the filament. The number of rings is larger for higher input pulse energies and the produced rings are more pronounced in the fs case.

In Fig. 4 is shown for comparison the calculated and measured radius of the laser beam along the propagation axis for input pulses of 450 fs, 2 mJ. The agreement is obvious showing well the existence of a filament propagating over about 4 m in air, having an almost constant diameter of about 150 μm. The nonlinear focus is shifted in front of the linear one by about 2.5 m.

Spatial repartitions of the fluence at two different distances along the propagation axis are presented in Fig. 5 for the case of 450 fs, 2 mJ pulses. In the first meters in front of the nonlinear focus one can observe rings merging inward to the beam center, as we have also seen in Fig. 3. The appearance of ring patterns can be seen on the burning spot of the laser beam on UV photographic paper recorded at the same distance (see insets in Fig. 5). On the experimental profile one can see that the rings are not really uniform but due to the modulational instability they break in many small filaments that later on coalesce to a single filament. The role of the modulational instability has been addressed recently by Tzortzakis et al. [25] in the case of fs IR filaments in air, also ring formation has been addressed recently by Chin et al. [26]. Once the filament is formed, the trend is reversed, and light rings merge outwards in agreement with the experimental measurements.

4.2. Ionization

Comparative simulation results of 450 fs long pulses at different input energies are presented in Fig. 6. The dotted lines represent the 2 mJ, the dashed lines the 5 mJ, and the solid lines the 7.5 mJ. In Fig. 6 are shown results on the laser beam

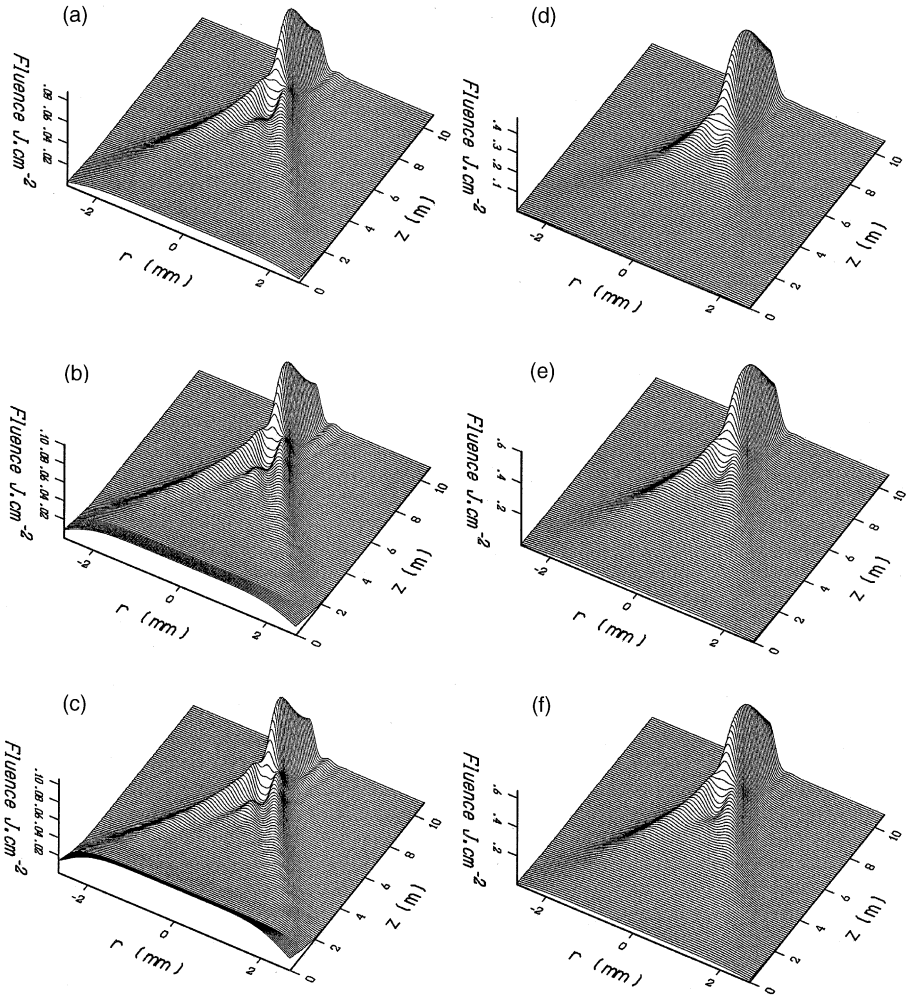

Fig. 3. Calculated fluence distributions along the propagation axis for fs pulses (first column) and ps pulses (second column). The first row is for input energy of 2 mJ, the second for 5 mJ and the third for 7.5 mJ.

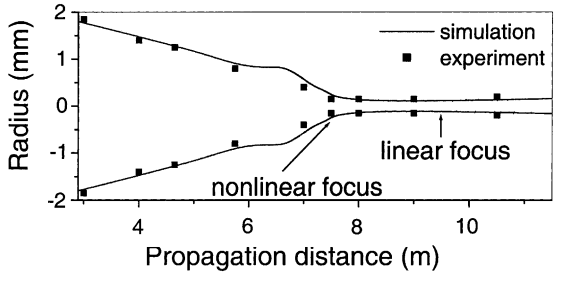

Fig. 4. Comparison between the measured (■) and calculated (—) beam profile in the case of 450 fs, 2 mJ pulses.

radius at FWHM, the maximum on axis ($r = 0$) fluence, and peak electron density from 7 to 11 m. For all the input energies considered here the results are very close, a filament is formed that propagates over many meters with a constant diameter of about 150 μm. The maximum fluence reaches 0.1 J/cm^2 and the maximum electron density reaches 10^{15} e$^-$/cm^3. This electron density is lower than the corresponding of IR fs filaments, which is about 10^{16} e$^-$/cm^3.

The same comparison as above is shown in Fig. 7 for 5 ps long pulses and for the same input pulse

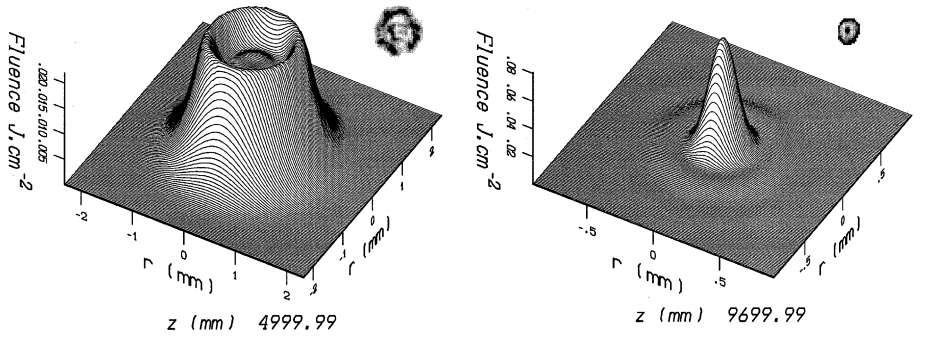

Fig. 5. Calculated spatial fluence distributions at two distances along the propagation axis. For comparison are also shown (small insets) measurements as recorded on UV photographic paper at the same distances. Observe the excellent agreement between the measurements and the simulations.

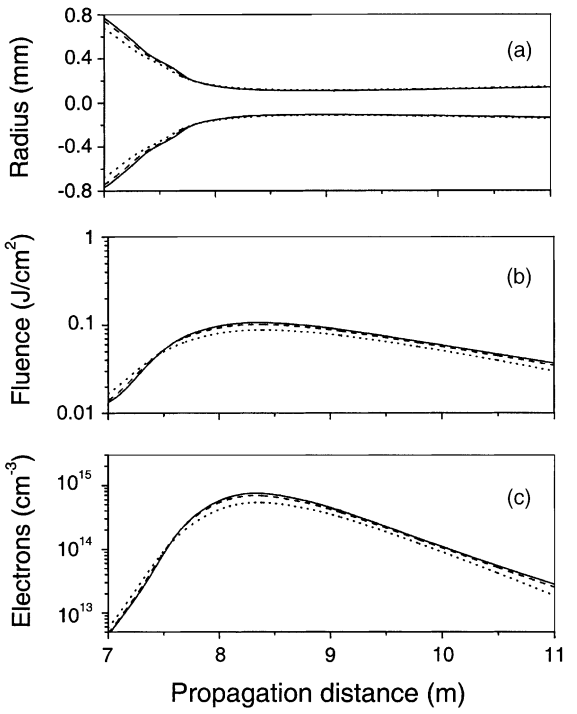

Fig. 6. Calculated beam radius (a), maximum on axis fluence (b), and peak electron density (c), along the propagation axis from 7 to 11 m. On those graphs results are shown for fs pulses with input energies of 2 mJ (···), 5 mJ (- - -) and 7.5 mJ (—).

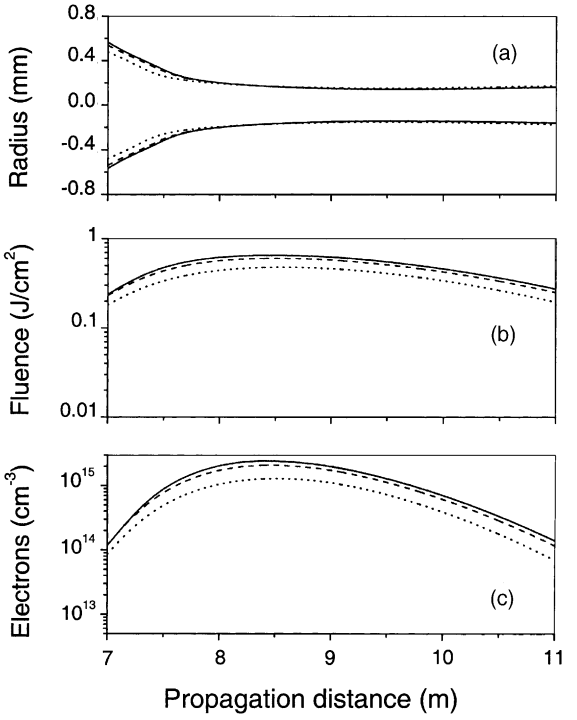

Fig. 7. Calculated beam radius (a), maximum on axis fluence (b), and peak electron density (c), along the propagation axis from 7 to 11 m. On those graphs results are shown for ps pulses with input energies of 2 mJ (···), 5 mJ (- - -) and 7.5 mJ (—).

energies as in Fig. 6. For the set of energies shown here the results are nearly the same, showing the existence of filaments propagating over many meters in air with constant diameter of about 200 μm, slightly larger than for fs filaments. The maximum fluence reaches almost 1 J/cm^2 and the maximum electron density exceeds 10^{15} e$^-$/cm^3. The factor 10 found when comparing the values of

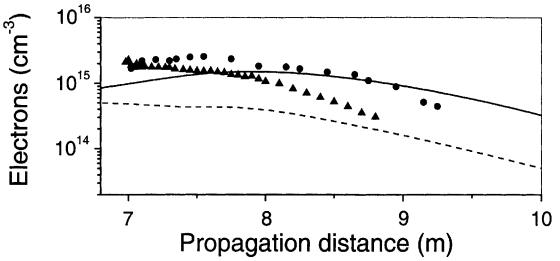

Fig. 8. Calculated and measured electron densities for 450 fs, 2 mJ pulses (dashed line and triangles respectively), and for 5 ps, 2 mJ pulses (solid line and squares respectively).

fluence in the case of 450 fs and 5 ps long pulses is directly related to the factor 10 difference in pulse duration, resulting in the same intensity in both cases in the filaments.

A comparison between the ionization in the fs filament and the ps filament is presented in Fig. 8. In dashed line is the calculated electron density for 450 fs, 2 mJ pulses, which is to be compared with the measurements represented by the triangles. The solid line is the calculated electron density for 5 ps, 2 mJ pulses, which is to be compared to the measurements represented by the circles. Both calculations and measurements show clearly that in the case of ps UV filaments the electron density is higher than for fs UV filaments.

In Fig. 9 the role of the different species of the air (O_2 and N_2) is demonstrated for both fs (Fig. 9a) and ps pulses (Fig. 9b), for input laser pulse energy of 5 mJ. The dotted lines represent the N_2 contribution, the dashed lines represent the O_2 contribution, and the solid lines represent air with the mixed contribution of oxygen and nitrogen. A first observation is the clear predominance of O_2 molecules ionization in the total electron density. Even if the N_2 molecules are in much higher proportion in air (80% compared to 20% for oxygen) this is an expected result because of the much lower ionization potential of oxygen compared to nitrogen. The electron density is slightly larger in the ps filaments than in the fs ones. Nevertheless the on axis electron density along the whole propagation distance from 0 to 11 m is much more uniform in the fs case, ranging over two orders of magnitude, than in the ps where the range is extended to four orders of magnitude.

Fig. 10 presents the ionization rate (ρ/ρ_{at}) as a function of r and z for fs pulses (Fig. 10a) and the ps pulses (Fig. 10b), for input laser energy of 2 mJ. Observing those two figures one can see the important contribution to the ionization of the initial spatial rings in the case of fs pulses. By contrast, in the case of ps pulses this contribution is negligible.

4.3. Pulse temporal and spectral evolution

Temporal autocorrelation measurements at different distances along the propagation of the laser beam are presented in Fig. 11 for fs pulses at two input laser pulse energies of 2 mJ (Fig. 11a) and 5 mJ (Fig. 11b). For comparison the measured initial laser pulse autocorrelation is also shown. For both energies the results are very close: the shortening of the central autocorrelation peak and the pedestal at the wings suggest break-up and compression of the initial pulse. The central peak

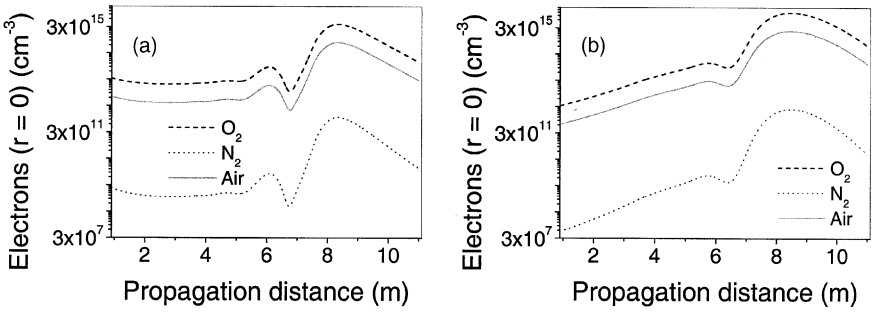

Fig. 9. Calculated electron densities for fs (a) and ps pulses (b) at input energy of 5 mJ. The respective contribution of N_2 (···) and O_2 (- - -), in the mixed air composition (—) is shown.

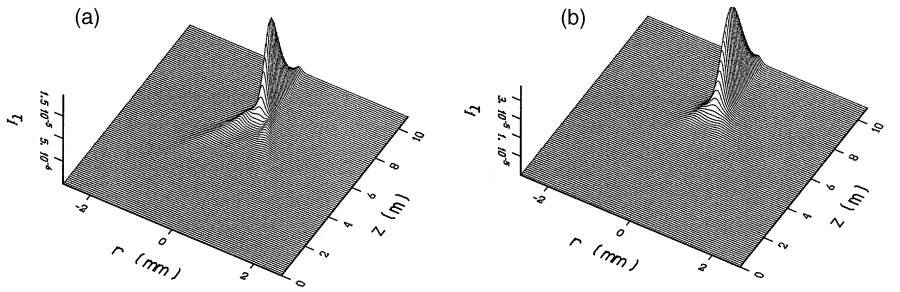

Fig. 10. Calculated image of the spatial (r) contribution of the ionization (ionization rate) along the propagation (z) in the fs (a) and ps case (b), for input pulse energy of 2 mJ.

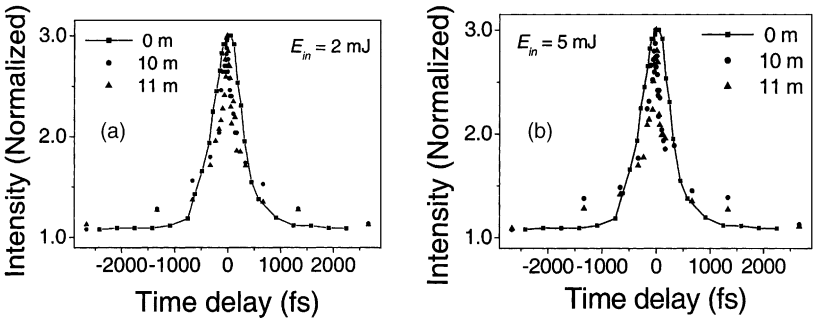

Fig. 11. Measured autocorrelation traces in fs filaments for two input energies of 2 mJ (a) and 5 mJ (b). Measurements at two different distances of 10 m (●) and 11 m (▲) are shown together with the initial pulse autocorrelation trace (—■—).

is about a factor two shorter than that of the initial pulse autocorrelation. This in turn suggests a consequent pulse compression of the order of 2. The stability of this structure over many meters of propagation is also remarkable, supporting the existence of a particular propagation mode.

In Fig. 12a and b the calculated pulse temporal profile in the filament is shown at two distances of the propagation. The initial pulse splits into two shorter sub-pulses, which propagate almost unchanged over about 4 m. In Fig. 12c and d autocorrelation traces resulting from the simulations are directly compared to the experimental measurements. The numerically calculated autocorrelation curves result from application of the formula (1). Results at two different distances in the filament are shown together with the initial pulse autocorrelation for both initial pulse energies. The simulations reproduce in a very good way the central peak of the experimentally obtained autocorrelations, while a discrepancy is observed in the wings. Unfortunately only few experimental points have been recorded in this region. This makes a direct comparison with simulations hardly meaningful. In the simulations the two peaks of the pulse structure have almost the same amplitude, which translates to high amplitude secondary peaks in the autocorrelation. On the other hand the experimental autocorrelations seem to show less pronounced secondary peaks, which probably indicates that the two peaks in the double pulse do not have the same amplitude. Nevertheless as we will show below a more convincing evidence that there is indeed formation of a double pulse is given by the characteristic fringe pattern in the power spectrum of the filament.

In Fig. 13 the pulse evolution along the propagation axis of the fs filament is shown, for input laser energy of 5 mJ. This figure clearly indicates that energy from the central part of the pulse nourish the filament and the two surrounding peaks. Once this energy reservoir is empty, after

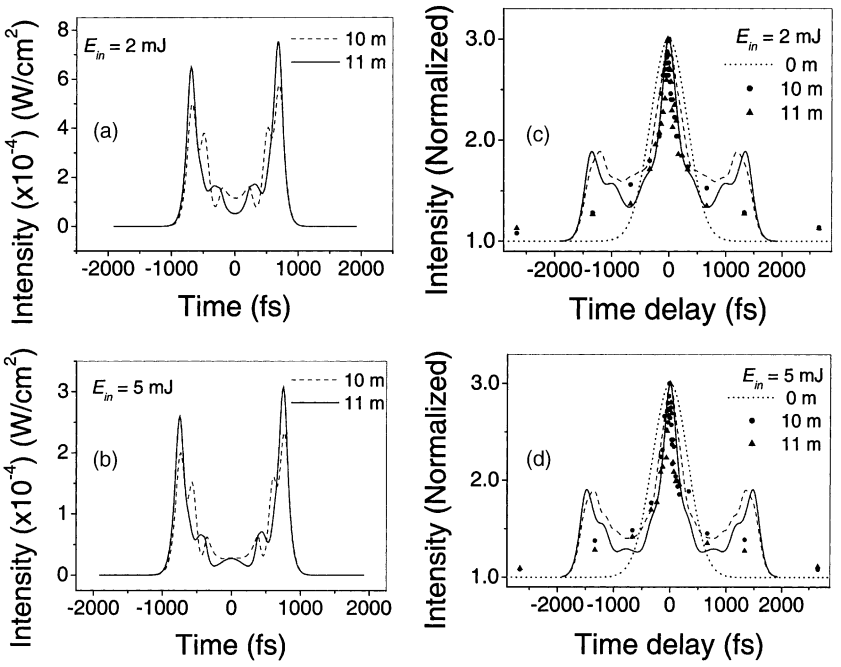

Fig. 12. Calculated pulse temporal profiles (a, b) and corresponding autocorrelations (c, d) in the fs filaments for input energies of 2 mJ (a, c) and 5 mJ (b, d). Results are shown for two distances of 10 m (- - -) and 11 m (—). In (c, d) is also shown the autocorrelation trace of the initial pulse (···) and the measured autocorrelations at 10 m (●) and 11 m (▲).

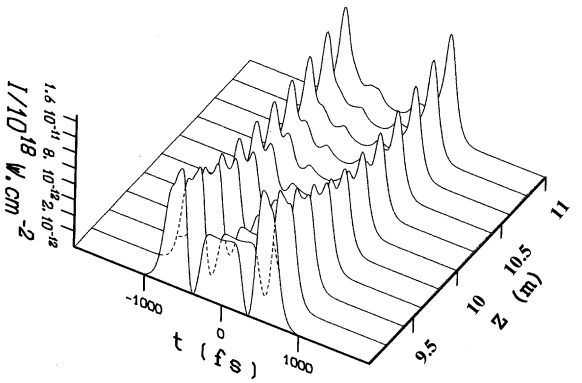

Fig. 13. Calculated pulse temporal profile evolution along the propagation axis from 9 to 11 m, for 5 mJ pulses with 450 fs initial duration.

11 m, the filament starts diffracting, as seen from the inspection of the spatial profile measurements and calculations shown, i.e. in Fig. 4.

In Fig. 14a the calculated pulse temporal profile in the ps filament is shown at 11 m together with the initial pulse (dotted line). The initial pulse splits into two shorter sub-pulses, which in this case do not have the same amplitude, as was the case with the fs filaments described above. In Fig. 14b the autocorrelation trace resulting from the simulation at 11 m is directly compared to the experimental measurement (triangles). The initial pulse autocorrelation is also shown in the same figure represented by the dotted line.

In Fig. 15 the pulse evolution along the propagation axis of the ps filament is shown, for input laser energy of 7.5 mJ. This figure clearly indicates that energy from the central part of the pulse nourish the filament and the two surrounding peaks. Moreover it shows that contrary to the fs case here the intensity distribution in the two peaks is not symmetric. Here it is the rear peak (positive times) that gains more energy from the center. As was the case with fs pulses, once this energy reservoir is empty, after 11 m, the filament starts diffracting.

Another way to verify the presence of a double peak structure is to compare the measured and

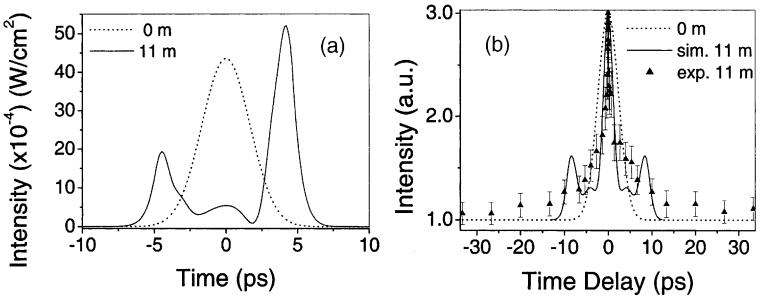

Fig. 14. Calculated pulse temporal profiles (a) and corresponding autocorrelations (b) in the ps filaments for input energy of 7.5 mJ. Results are shown at 11 m (—) together with the initial pulse (···). In (b) is also shown the measured autocorrelation at 11 m (▲).

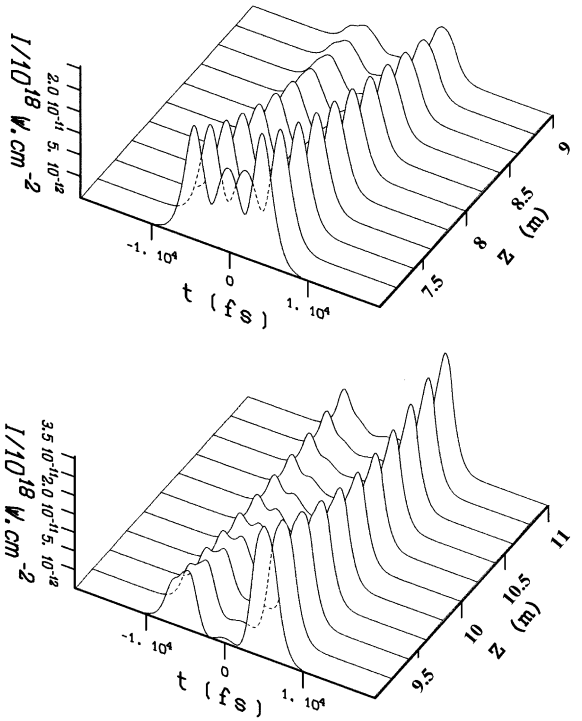

Fig. 15. Calculated pulse temporal profile evolution along the propagation axis from 7 to 11 m, for 7.5 mJ pulses with 5 ps initial duration.

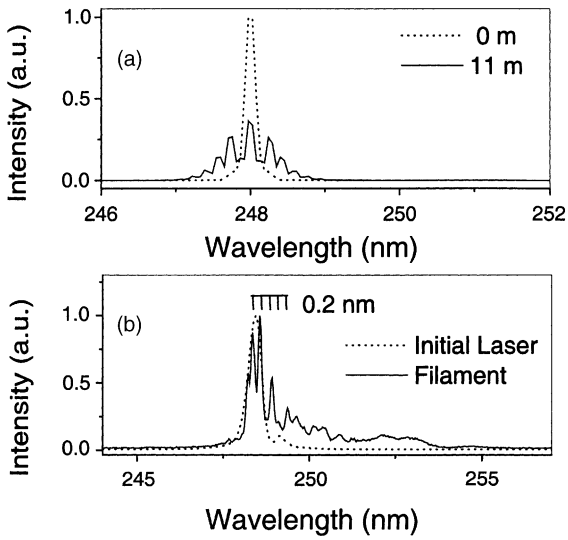

Fig. 16. Calculated (a) and measured spectra (b) for 450 fs, 5 mJ pulses. The initial pulse is in dotted line and the filament at 11 m is in solid. Both calculated and measured spectra in the filament have a fringe structure with an inter-fringe space of 0.2 nm.

simulated power spectra. The numerically produced double pulse structure in the fs filament has a power spectrum (Fig. 16a) with a characteristic fringe pattern with an inter-fringe space of about 0.2 nm. This is in good agreement with the measurement presented in Fig. 16b. The same comparison in the case of ps pulses, shown in Fig. 17, does not clearly indicate the existence of fringes in the spectrum, which is also in agreement with the measurements and the nonsymmetrical pulse structure in the ps filament.

In Fig. 18 more spectra are shown for the case of fs pulses at two input energies of 2 mJ (Fig. 18a) and 5 mJ (Fig. 18b). The spectra are plotted on a logarithmic scale and show measurements at different distances of the propagation. One can observe that the spectral broadening exists only in the filament. Moreover the shape of the spectra in the filament stays quite stable being another proof of

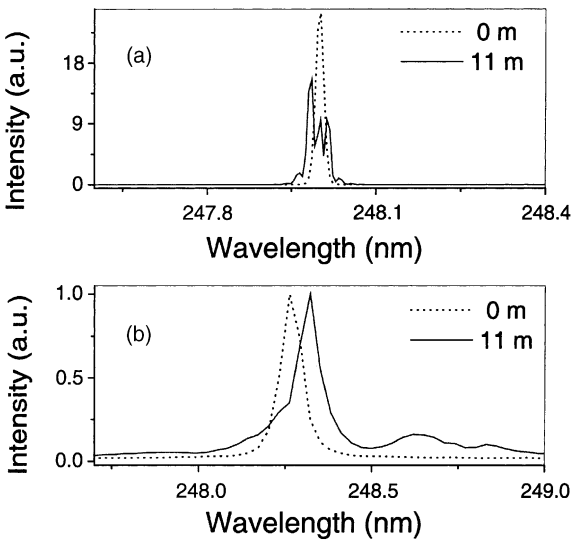

Fig. 17. Calculated (a) and measured spectra (b) for 5 ps, 7.5 mJ pulses. In dotted line in the initial pulse and in solid the filament at 11 m.

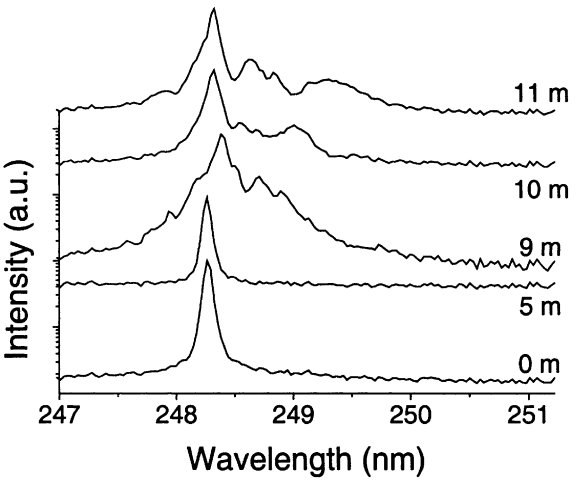

Fig. 19. Measured power spectra at different distances along the propagation axis for 5 ps initial pulses with input energy of 7.5 mJ. The y-axis is in logarithmic scale. Notice the stable spectral structure in the filaments (9, 10, 11 m).

the stability and the existence of a special propagation mode. Similar are the conclusions as it concerns ps filaments the spectra of which are shown in Fig. 19.

Two general remarks can be made about the reported measured spectra. First, the observed spectral broadening is significantly smaller than for IR filaments. This is due to the almost two orders of magnitude lower intensity in the UV filaments as compared to the IR ones. This is the result of the much higher ionization cross-sections of the ultraviolet radiation as compared to the infrared one. Thus the laser intensity needed to obtain a certain threshold value of the electronic density is lower. The second remark is that the

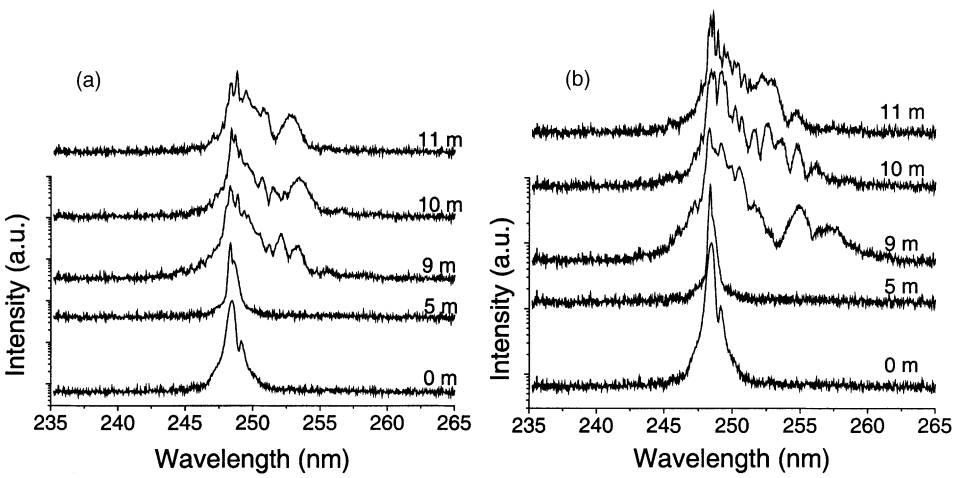

Fig. 18. Measured power spectra at different distances along the propagation axis for 450 fs initial pulses with input energy of 2 mJ (a) and 5 mJ (b). The y-axis is in logarithmic scale. Notice the stable spectral structure in the filaments (9, 10, 11 m).

spectrum's center of gravity shifts slightly towards lower energies. This is opposite to what is observed in the IR filamentation. A possible explanation to this could be the relatively long pulse durations used in this study (450 fs and 5 ps) as compared to the IR filamentation. Gaeta [21] has attributed the spectral shift, towards higher energies, in the IR fs ($\sim$100 fs) filamentation to important pulse steepening effects giving rise to very sharp and spiky structures. In the present case such pulse steepening effects are not observed due to the initially longer pulses and the lower intensities in the filament.

5. Conclusion

In conclusion, we have presented a detailed experimental and numerical study on the nonlinear propagation of short (femtosecond and picosecond) UV pulses in air. Long-range beam filamentation has been observed with both fs and ps pulses. The filament characteristics are similar in both regimes; a slightly larger diameter and more electrons are produced for the ps as compared to the fs filament. In both cases the initial pulse breaks down to two sub-pulses with shorter duration. In the fs case the two sub-pulses seem to be symmetric while in the ps case the rear sub-pulse dominates over the leading one. The pulse splitting is promoted mainly by MPI. This break-up is of great importance in the formation and propagation of the filament, as it seems to play the role of a spatio-temporal waveguide.

Acknowledgements

We kindly acknowledge the assistance of A. Eglezis in the experimental procedure. We also thank A. Couairon for fruitful discussions. This study was made possible through the access to the Ultraviolet Laser Facility operating at FORTH-IESL under the "Improving Human Potential-Access to Research Infrastructures" Programme (contract no: HPRI-CT 1999-00074) of the EU.

References

[1] A. Braun, G. Korn, X. Liu, D. Du, J. Squier, G. Mourou, Opt. Lett. 20 (1995) 73–75.
[2] E.T.J. Nibbering, et al., Opt. Lett. 21 (1996) 62–64.
[3] A. Brodeur, C.Y. Chien, F.A. Ilkov, S.L. Chin, O.G. Kosareva, V.P. Kandidov, Opt. Lett. 22 (1997) 304–306.
[4] H. Schillinger, R. Sauerbrey, Appl. Phys. B 68 (1999) 753–756.
[5] S. Tzortzakis, et al., Phys. Rev. E 60 (1999) R3505–R3507.
[6] S. Tzortzakis, B. Prade, M. Franco, A. Mysyrowicz, Opt. Commun. 181 (2000) 123–127.
[7] B. La Fontaine, et al., Phys. Plasmas 6 (1999) 1615–1621.
[8] D. Comtois, et al., Appl. Phys. Lett. 76 (2000) 819–821.
[9] A. Talebpour, S. Petit, S.L. Chin, Opt. Commun. 171 (1999) 285–290.
[10] M. Mlejnek, E.M. Wright, J.V. Moloney, Opt. Lett. 23 (1998) 382–384.
[11] A. Chiron, et al., Eur. Phys. J. D 6 (1999) 383–396.
[12] A. Couairon, L. Bergé, Phys. Plasmas 7 (2000) 193–209.
[13] A. Talebpour, M. Abdel-Fattah, S.L. Chin, Opt. Commun. 183 (2000) 479–484.
[14] M. Mlejnek, M. Kolesik, J.V. Moloney, E.M. Wright, Phys. Rev. Lett. 83 (1999) 2938–2941.
[15] N. Aközbek, C.M. Bowden, A. Talebpour, S.L. Chin, Phys. Rev. E 61 (2000) 4540–4549.
[16] I.G. Koprinkov, A. Suda, P. Wang, K. Midorikawa, Phys. Rev. Lett. 84 (2000) 3847–3850.
[17] L. Bergé, A. Couairon, Phys. Rev. Lett. 86 (2001) 1003–1006.
[18] J. Schwarz, P. Rambo, J.-C. Diels, M. Kolesik, E.M. Wright, J.V. Moloney, Opt. Commun. 180 (2000) 383–390.
[19] S. Tzortzakis, et al., Opt. Lett. 25 (2000) 1270–1272.
[20] S. Szatmari, F.P. Schäfer, Opt. Commun. 68 (1988) 196–202.
[21] A.L. Gaeta, Phys. Rev. Lett. 84 (2000) 3582–3585.
[22] A. Zozulya, S.A. Diddams, A.G. Van Engen, T.S. Clement, Phys. Rev. Lett. 82 (1999) 1430–1433.
[23] L.V. Keldysh, Sov. Phys. JETP 20 (1965) 1307–1314.
[24] J.-F. Ripoche, et al., Opt. Commun. 135 (1997) 310–314.
[25] S. Tzortzakis, L. Bergé, A. Couairon, M. Franco, B. Prade, A. Mysyrowicz, Phys. Rev. Lett. 86 (2001) 5470–5473.
[26] S.L. Chin, N. Aközbek, A. Proulx, S. Petit, C.M. Bowden, Opt. Commun. 188 (2001) 181–186.